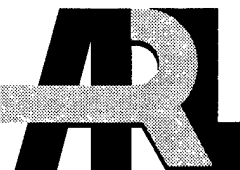


ARMY RESEARCH LABORATORY



# Loss of Rate Capability in $\text{LiMn}_2\text{O}_4$ /Carbon Cells

Jeffrey Read, Jeff Wolfenstine, Donald Foster, and Wishvender Behl

ARL-TR-2115

March 2000

Approved for public release; distribution unlimited.

The findings in this report are not to be construed as an official Department of the Army position unless so designated by other authorized documents.

Citation of manufacturer's or trade names does not constitute an official endorsement or approval of the use thereof.

Destroy this report when it is no longer needed. Do not return it to the originator.

# Army Research Laboratory

Adelphi, MD 20783-1197

---

ARL-TR-2115

March 2000

---

## Loss of Rate Capability in $\text{LiMn}_2\text{O}_4$ /Carbon Cells

Jeffrey Read, Jeff Wolfenstine, Donald Foster, and Wishvender Behl

Sensors and Electron Devices Directorate

---

Approved for public release; distribution unlimited.

---

---

## Abstract

---

We present a survey of the available literature on the loss in rate capability of  $\text{LiMn}_2\text{O}_4$ -based lithium-ion batteries. Manganese dissolution is identified as the main cause of rate capability loss, as well as loss in capacity during storage. Manganese dissolution results in passivation of both the cathode and anode, structural changes at the spinel surface, and loss in particle contact. Manganese dissolution can be reduced by surface treatments, increased electrolyte stability, and removal of acidic protons from the electrolyte.

## Contents

|  |           |
|--|-----------|
| <b>1. Introduction .....</b>   | <b>1</b>  |
| <b>2. <math>\text{LiMn}_2\text{O}_4</math> Background .....</b>            | <b>2</b>  |
| 2.1 Structure .....  | 2         |
| 2.2 Preparation .....  | 2         |
| 2.3 3- and 4-V Discharge Regions .....                                     | 2         |
| 2.4 Capacity Fade .....  | 3         |
| 2.5 Self-Discharge in Storage .....  | 4         |
| <b>3. Loss of Rate Capability .....</b>                                    | <b>6</b>  |
| 3.1 During Cycling .....   | 6         |
| 3.2 After Storage in the Discharged State .....                            | 8         |
| 3.3 After Storage .....  | 10        |
| <b>4. Summary .....</b>  | <b>13</b> |
| <b>5. Improving Rate Capability After Storage and During Cycling .....</b> | <b>14</b> |
| 5.1 Reduced Surface Area .....   | 14        |
| 5.2 Surface Treatments .....   | 14        |
| 5.3 Trapping HF/Water Removal .....  | 15        |
| <b>6. Conclusions .....</b>  | <b>16</b> |
| <b>References .....</b>  | <b>17</b> |
| <b>Distribution .....</b>  | <b>19</b> |
| <b>Report Documentation Page .....</b>                                     | <b>21</b> |

# 1. Introduction

$\text{LiMn}_2\text{O}_4$  spinel has been one of the most widely studied cathode materials for use in lithium-ion batteries in recent years [1–3]. The current generation of lithium-ion batteries uses  $\text{LiCoO}_2$  cathodes and various forms of carbon as anodes.  $\text{LiCoO}_2$  is the only cathode material in wide commercial use today. The high cost of cobalt led to the study of alternative materials, and  $\text{LiMn}_2\text{O}_4$  is now seen as an excellent replacement because of its low cost and ease of preparation.

$\text{LiMn}_2\text{O}_4$  spinel has not been commercialized to date because of its poor cycling performance and poor storage at elevated temperature. The poor performance has been linked to several problems, including electrolyte oxidation, manganese dissolution, and distortion of the crystal lattice due to the Jahn-Teller effect on deep discharge.

In this report, we summarize the available literature and detail the remedies suggested to improve  $\text{LiMn}_2\text{O}_4$  performance. We give evidence that links poor storage and cycling performance to a loss in rate capability of the spinel.

## 2. $\text{LiMn}_2\text{O}_4$ Background

### 2.1 Structure

The structure of  $\text{LiMn}_2\text{O}_4$  is that of a cubic spinel of space group  $Fd3m$ . The structure consists of a cubic, close-packed oxygen array with the oxygen anions on the  $32e$  sites of the  $Fd3m$  space group, with  $\text{Mn}^{+3}$  and  $\text{Mn}^{+4}$  ions occupying the  $16d$  octahedral positions, and  $\text{Li}^+$  occupying the  $8a$  tetrahedral sites [4]. The  $\text{Mn}_2\text{O}_4$  network defines a three-dimensional (3-D) space for lithium ion diffusion. Empty tetrahedral ( $8a$ ) and octahedral ( $16c$ ) sites that share faces create a 3-D tunnel structure that allows lithium ions to move easily through the structure.

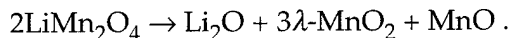
### 2.2 Preparation

Wickham and Croft first described the preparation of  $\text{LiMn}_2\text{O}_4$  spinel in 1958 [5].  $\text{LiMn}_2\text{O}_4$  is most often prepared by intimate mixing of  $\text{MnO}_2$  and  $\text{Li}_2\text{CO}_3$  in a high intensity mixer or ball mill. The powder is then heated at 790 to 800 °C for several hours. Repeated grinding with subsequent heating at 790 to 800 °C improves crystallinity and helps complete the reaction. The bluish-black powder can be formulated as  $\text{Li}^+\text{Mn}^{+3}\text{Mn}^{+4}\text{O}_4$ .  $\text{LiMn}_2\text{O}_4$  spinel has also been prepared by sol-gel techniques [6] at temperature  $T < 400$  °C, by the Pechini process [7] and by reactive electron-beam evaporation [8].

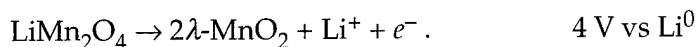
The material properties and preparation conditions have a strong influence on spinel performance. Grain size [1], crystallinity [6,9,10], oxygen content [11,12], defect structure [13], stoichiometry [14], firing temperature [1,12], cooling rate [12], and oxygen partial pressure [15,16] have all been shown to affect cycling performance and the capacity of this material.

### 2.3 3- and 4-V Discharge Regions

Hunter [17] first described the chemical extraction of lithium from  $\text{LiMn}_2\text{O}_4$  spinel using acid treatment. The material formed by lithium extraction,  $\lambda\text{-MnO}_2$ , is simply the spinel framework void of lithium:

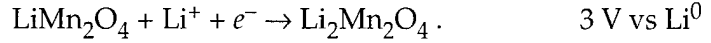


Thackeray et al [3] first described the electrochemical extraction of lithium from  $\text{LiMn}_2\text{O}_4$  in 1-M  $\text{LiBF}_4$ /propylene carbonate electrolyte to form  $\lambda\text{-MnO}_2$ . This extraction takes place at 4 V versus lithium and involves the removal of lithium ions from tetrahedral sites:



The maximum theoretical charge capacity over the 4-V plateau is 148 mAh/g, with capacities of 125 mAh/g typically realized.

Thackeray et al [18] also described the insertion of lithium at 3 V into  $\text{LiMn}_2\text{O}_4$  in 1-M  $\text{LiBF}_4$ /propylene carbonate electrolyte:



The maximum theoretical discharge capacity over the 3-V plateau is 148 mAh/g.

Ohzuku et al [2] described in detail the phase changes that occur as  $\lambda\text{-MnO}_2$  is lithiated, first to  $\text{LiMn}_2\text{O}_4$  and then to  $\text{Li}_2\text{Mn}_2\text{O}_4$ :

1. From  $0 < x < 0.6$  in  $\text{Li}_x\text{Mn}_2\text{O}_4$ , two cubic phases with lattice constants  $a_c = 8.045 \text{ \AA}$  and  $a_c = 8.142 \text{ \AA}$  coexist, and a constant open-circuit voltage of 4.110 V is observed.
2. From  $0.6 < x < 1.0$  in  $\text{Li}_x\text{Mn}_2\text{O}_4$ , a single homogeneous phase exists, with a continuous lattice expansion from  $a_c = 8.142 \text{ \AA}$  to  $a_c = 8.239 \text{ \AA}$ . The open-circuit voltage is S-shaped, with a midpoint of 3.94 V.
3. From  $1.0 < x < 2.0$  in  $\text{Li}_x\text{Mn}_2\text{O}_4$ , cubic and tetragonal phases coexist, and a constant open-circuit voltage of 2.957 V is observed. The cubic phase is  $\text{Li}_{1.0}\text{Mn}_2\text{O}_4$  with  $a_c = 8.239 \text{ \AA}$ , while the tetragonal phase is  $\text{Li}_{2.0}\text{Mn}_2\text{O}_4$  with  $a_T = 5.649 \text{ \AA}$  and  $c_T = 9.253 \text{ \AA}$ . The cubic-to-tetragonal phase transition occurs as a result of the Jahn-Teller distortion when more than half of the manganese is in the  $\text{Mn}^{+3}$  state.

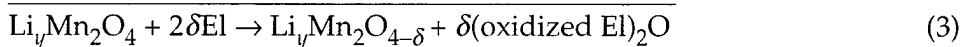
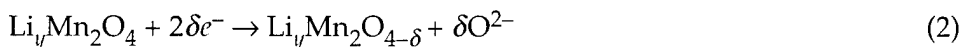
Cycling lithium over both the 3- and 4-V plateaus results in severe capacity fade due to destruction of the crystal lattice from Jahn-Teller distortion, which occurs when  $\text{Mn}^{+4}$  is reduced to  $\text{Mn}^{+3}$ .

## 2.4 Capacity Fade

Stoichiometric  $\text{LiMn}_2\text{O}_4$  has been found to have a slight capacity fade on cycling [11]. Possible causes of this observed behavior are [14]

- electrolyte oxidation at high voltage,
- dissolution of manganese, according to the reaction  $2\text{Mn}^{+3} \rightarrow \text{Mn}^{+2} + \text{Mn}^{+4}$ , or
- destruction of the lattice due to Jahn-Teller distortion on discharge.

Gao et al [19] demonstrated that capacity fading could be correlated to growth of a 3.3-V peak in the discharge curve of the spinel. Gao had previously demonstrated that this 3.3-V peak was attributable to oxygen deficiency in the spinel [16]. The growth of this 3.3-V peak was accentuated by charging the electrode to high voltages. Gao et al proposed a mechanism that involved the oxidation of electrolyte with simultaneous loss of oxygen from the spinel that could account for this behavior:





This reaction occurs at the surface of the spinel particle. Capacity fading from this mechanism results from structural damage to the surface of the spinel particle and electrolyte oxidation.

Jang et al [20,21] measured capacity fade and the dissolution of manganese and lithium as a function of applied potential, carbon content in the cathode, and electrolyte formulation. They demonstrated that manganese dissolution increased with cathode voltage and with cathode carbon content. Using various combinations of solvents and salts, Jang et al showed that manganese dissolution correlated directly with the ease of electrolyte oxidation and proton generation from that oxidation. An interesting experiment was conducted where a spinel electrode was left at open-circuit, while a nearby carbon electrode was held at 4.2 V. This experiment resulted in manganese dissolution at the open-circuit spinel electrode. Jang et al suggested that manganese and lithium dissolution results from acid attack. This acid is produced by oxidation of electrolyte solvents at the cathode surface, with additional acids being generated by decomposition of electrolyte salts from water contamination. The acid attack leads to the formation (at the surface of the spinel particle) of a defect spinel deficient in either manganese or lithium. Further acid attack destabilizes the lattice such that oxygen ions are depleted from the lattice. Jang et al reported that capacity fade resulted from two factors: manganese dissolution or capacity loss from cathode polarization. (Capacity loss was said to result from increased contact resistance between spinel and carbon particles.) The mechanism for manganese or lithium dissolution via acid attack was not specified.

It has been demonstrated that the cycling stability of  $\text{LiMn}_2\text{O}_4$  can be improved by doping the spinel with small levels of excess lithium, magnesium, or zinc [22,14].  $\text{Li}_{1+x}\text{Mn}_{2-x}\text{O}_4$ , where  $x > 0$ , shows increased cycling stability versus the stoichiometric material. The excess lithium ions are said to occupy manganese sites in the spinel structure [12]. The increase in stability is attributed to relief of effects from the Jahn-Teller distortion, as increased lithium content raises the mean oxidation state of manganese above 3.5. However, the doping of cations into the spinel lattice has the detrimental effect of decreasing capacity.

The cycling stability is also improved by cooling the spinel during synthesis from 800 to 500 °C at a rate not greater than 10 °C per hour [22]. This cooling rate ensures that the spinel is fully oxygenated and that, again, the average manganese valance is above 3.5.

## 2.5 Self-Discharge in Storage

$\text{LiMn}_2\text{O}_4$  has been found to have a significant self-discharge in storage at both room and elevated temperatures [23–25]. Suggested explanations for the self-discharge include

- electrolyte oxidation caused by high-surface-area materials in the cathode, resulting in both irreversible and reversible capacity loss, and
- manganese dissolution at high voltage, leading to irreversible capacity loss due to structural degradation.

Guyomard et al [24] investigated self-discharge in the  $\text{Li}_x\text{Mn}_2\text{O}_4$ /carbon system in both 1-M  $\text{LiClO}_4$  1:1 v/v (volume to volume) ethylene carbonate (EC):diethoxyethane (DEE) and 1-M  $\text{LiPF}_6$  1:2 v/v EC:dimethyl carbonate (DMC) electrolytes. Reversible self-discharge was measured as a function of carbon loading in the cathode at up to 5 V. Guyomard et al concluded that this self-discharge resulted from the oxidation of electrolyte and subsequent lithium intercalation into the delithiated spinel. Electrolyte oxidation scaled with carbon loading, so the researchers concluded that solvent oxidation occurred mainly on the carbon additive in the cathode, and that self-discharge could be limited by reducing the carbon loading to the minimum needed for reasonable electrode conductivity. Irreversible capacity loss was not addressed.

Amatucci et al [25] studied the effects of a host of material properties on spinel self-discharge in the charged state. The material properties studied included morphology, defects, surface area, structural instability, single versus two-phase lithium-insertion processes, cation and oxygen stoichiometry, and manganese solubility. The material property determined to have the largest effect on capacity loss, both reversible and irreversible, was spinel surface area. Increasing surface area from 0.6 to 3.5  $\text{m}^2/\text{g}$  increased both reversible and irreversible capacity loss by a factor of three. Increased spinel surface area was also shown to scale with manganese dissolution. A specific mechanism was not proposed to account for the observed self-discharge, although electrolyte oxidation and manganese dissolution were noted as being clearly related to the phenomenon.

Blyr et al [26] investigated self-discharge in the  $\text{LiMn}_2\text{O}_4$ /1-M  $\text{LiPF}_6$  in 2:1 v/v EC:DMC/carbon system in the discharged state. Three electrode measurements were used to determine the source of poor self-discharge characteristics. Storage of Swagelok<sup>TM</sup>-type cells in the discharged state at 55 °C demonstrated losses in cell capacity of as high as 20 percent per week. Storage of Bellcore PliON<sup>TM</sup> cells in the discharged state at 55 °C led to losses in cell capacity of as high as 15 percent per week. Blyr et al concluded that self-discharge was caused by several factors:

- Self-discharge at the anode as the result of solid electrolyte interface growth.
- Self-discharge at the anode from the reduction of soluble manganese.
- Self-discharge at the cathode via a cation exchange reaction between manganese and lithium that results in manganese dissolution.

### 3. Loss of Rate Capability

#### 3.1 During Cycling

Jang et al [20] investigated manganese dissolution and impedance growth in  $\text{Li}^0/1\text{-M LiClO}_4$  in 1:1 PC:dimethoxyethane (DME)/ $\text{Li}_{1.0}\text{Mn}_2\text{O}_4$  cells as a function of carbon loading, heat treatment temperature, and cathode potential. Cathodes were prepared by mixing spinel powders with acetylene black (Vulcan XC-72) and Teflon binder at various percentages. The mixtures were dispersed in isopropyl alcohol and pasted onto Exmet screen, pressed, and dried at  $120^\circ\text{C}$  for 3 hr. Cells were cycled from 3.6 to 4.3 V at  $1\text{ mA/cm}^2$ . Discharge curves and impedance spectra were taken as a function of cycle number for 21-, 30-, and 37-percent carbon-loaded electrodes.

Manganese dissolution was higher with increased carbon loading in the cathode. Lower surface area spinels prepared at  $800^\circ\text{C}$  showed less manganese dissolution than higher surface area materials calcined at  $600^\circ\text{C}$ . Holding the cathode at higher potentials increased dissolution. Holding a carbon electrode at 4.2 V in the near vicinity of an open-circuit spinel electrode increased dissolution. Jang et al proposed that manganese dissolution is induced by some intermediate generated by electrochemical oxidation of electrolyte on carbon particle surfaces.

Plots of discharge capacity versus carbon loading demonstrated that increased carbon loading leads to better cell capacity and better rate capability. Cell polarization was obvious from the charge and discharge curves for the 21-percent carbon-loaded cathode, while polarization in the 37-percent carbon-loaded cathode was not noticeable. The ac impedance spectra taken at 0, 20, 31, and 40 cycles determined that both  $R_{\text{contact}}$  (the resistance between the spinel particles and the carbon conductor) and  $R_{\text{el}}$  (the resistance for electrode reactions) grew as a function of cycle number, with the higher loaded cathodes growing less.

Jang et al proposed a mechanism to explain the rate capability/capacity loss data. Manganese dissolution can have two effects on the cell:

1. Loss in rate capability caused by loss in contact between spinel particles and the carbon conductor as the spinel dissolves. This is most severe in cathodes with lower carbon contents.
2. Loss in capacity caused by loss in active manganese. This effect is most noticeable in cathodes with higher carbon contents.

No specific chemical pathway was proposed for manganese dissolution, although the disproportionation reaction



was ruled out because dissolution was found to take place predominantly at the end of charge, when  $\text{Mn}^{+3}$  concentration is minimal.

Jang et al [21] extended the investigation of manganese dissolution and impedance growth in  $\text{Li}^0/\text{Li}_{1.0}\text{Mn}_2\text{O}_4$  cells, discussed in section 3.1, to include the effects of electrolyte formulation. Cells were constructed with the same techniques discussed above. Various electrolyte solvent systems and salts were tested with spinel cathodes under continuous cycling conditions, under open circuit and during float charge at 4.2 V. Cells were cycled from 3.6 to 4.3 V at 1 mA/cm<sup>2</sup>.

Manganese dissolution was clearly related to electrolyte formulation. Several factors governed how the spinel performed in the presence of different electrolytes.

The first relationship that emerged was between electrolyte oxidation potential on a carbon electrode and the concentration of manganese in solution as a spinel electrode was cycled. Electrolytes that oxidized at lower potentials gave rise to larger manganese dissolution. Proton-selective membrane glass electrode measurements in electrolytes with a 4.2-V polarized (vs  $\text{Li}/\text{Li}^+$ ) carbon electrode demonstrated that proton generation scaled with ease of electrolyte oxidation and with manganese dissolution. The  $\text{LiClO}_4$  electrolytes tested showed proton generation and manganese dissolution in the order

$$\text{PC:THF} > \text{PC:DME} > \text{EC:DEC} > \text{PC:DEC} .$$

The second relationship demonstrated was the effect of electrolyte salt on manganese dissolution. Proton concentration measured with a proton-selective membrane glass electrode demonstrated that in fresh PC/DME electrolytes, without the influence of a polarized carbon electrode, the proton concentration ordered as

$$\text{LiPF}_6 > \text{LiBF}_4 > \text{LiAsF}_6 > \text{LiClO}_4 > \text{LiCF}_3\text{SO}_3 ,$$

with manganese dissolution following the same trend. This effect is the result of water and hydrofluoric acid (HF) contamination in the salts as received, with the  $\text{LiPF}_6$  and  $\text{LiBF}_4$  salts having the highest water and HF concentrations when received. When a carbon electrode was charged to 4.2 V in the presence of each electrolyte, the protons generated from electrolyte oxidation showed the following trend:

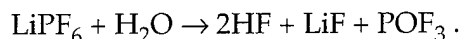
$$\text{LiCF}_3\text{SO}_3 > \text{LiClO}_4 > \text{LiAsF}_6 > \text{LiBF}_4 > \text{LiPF}_6 .$$

This same trend was found when the solvent oxidation was measured under stepped potential at 4.2 V with a carbon electrode. When both the trend of water and HF contamination in fresh electrolyte and the ease of oxidation as a function of electrolyte formulation were coupled, the extent of manganese dissolution followed the trend

$$\text{LiCF}_3\text{SO}_3 > \text{LiPF}_6 > \text{LiClO}_4 > \text{LiAsF}_6 > \text{LiBF}_4 .$$

The  $\text{LiPF}_6$  electrolyte deviated from the measurements of proton concentration, demonstrating greater manganese dissolution than expected. This

is explained by the ease with which this salt reacted with water from the following reaction:



The conclusion of this report is that manganese dissolution has a direct effect on rate capability, since dissolution inevitably leads to a loss in contact between the carbon added for conductivity and the spinel.

### 3.2 After Storage in the Discharged State

Blyr et al [26] measured the potential distribution through Bellcore PliON™ plastic lithium-ion cells to determine the source of poor electrochemical performance at elevated temperatures. Three- and four-electrode cells were used to monitor state of charge, polarization, and rate capability in both the anode and cathode under various conditions.

Cells were built with spinels of nominal composition  $\text{Li}_{1.05}\text{Mn}_2\text{O}_4$ , synthesized by either a slow-cooling (SC) or quenching (Q) process. The quenched samples are electrochemically different from the slow-cooled samples in that they show two extra peaks at 3.3 and 4.5 V in their cyclic voltammogram [12]. Anodes consisted of either MCMB-2510 or MCMB-2528, a disordered carbon and graphitized carbon, respectively. 1-M  $\text{LiPF}_6$  in 2:1 v/v EC:DMC was used as the electrolyte. Bellcore PliON™ electrodes [27] were prepared and used in either Swagelok™-type cells or Bellcore PliON™ cells. Lithium metal reference electrodes were mainly used for the reference electrode work, with  $\text{Li}_{4+x}\text{Ti}_5\text{O}_{12}$  used occasionally in the four-electrode cells. Cells were subjected to a variety of cycling, power, and self-discharge tests at rates of C/8 to 2C. Most cycling was carried out at the C/5 rate.

Cells tested with current interrupt methods (galvanic intermittent titration technique, GITT) revealed that even in fresh cells, the spinel cathode is more rate limiting than the carbon anode. When a cell is cycled at 55 °C, the cathode polarization increases from 50 mV for a fresh cell to 400 mV after 100 cycles. The anode polarization does not increase. The capacity at C/5 fades to 65 percent of its initial value after 100 cycles at 55 °C. These experiments point to the spinel as the source of poor performance.

Storage of Swagelok™-type cells in the discharged state at 55 °C led to losses in cell capacity as high as 20 percent per week. Cathode potentials dropped to 3.0 V (SC) or 3.3 V (Q) upon storage, indicating further reduction of the spinel. Anode potentials quickly rose to >2.5 V versus  $\text{Li}^0$  upon storage, and when anode potentials rose to >3.2 V, the battery did not recharge. A 2-V shift in the lithium reference potential was found to occur quite often after one week of storage at 55 °C, with manganese found on the lithium reference electrode and carbon anode via energy dispersive spectroscopy (EDS) and atomic absorption (AA) spectroscopy. Cells that could cycle after storage showed increased polarization in both the anode and cathode, with the anode polarization growing the most. Cathodes

and anodes removed from poorly cycling cells stored for one week at 55 °C were placed in half cells versus lithium. The cathodes showed a 25-percent capacity loss and an increased polarization from fresh electrodes. The anodes could not sustain capacity until washed with a  $\text{H}_2\text{O}_2/\text{HNO}_3/\text{H}_2\text{O}$  solution, whereupon they regained normal capacity and the ability to hold that capacity. All these results were explained as the consequences of manganese dissolution from the spinel:

1. Manganese dissolution leads to capacity loss in the spinel via loss of manganese.
2. Manganese poisoning of the carbon anode results in an inability of the carbon anode to cycle versus lithium.
3. Manganese poisoning of the carbon leads to an increased anode polarization, even after treatment with a peroxide/acid/water etch.
4. Manganese poisoning of the lithium reference causes a 2-V shift in reference potential.

The increase in cathode polarization was not explained in terms of the manganese dissolution.

Bellcore PliON™ cells were built and cycled at 25 °C. The cathode showed a slight increase in polarization after 100 cycles. Power rate testing, carried out on these plastic cells after 200 cycles, demonstrated that the rate capability is limited by the spinel cathode. These experiments point to the spinel as the source of poor performance.

Storage of Bellcore PliON™ cells in the discharged state at 55 °C led to losses in cell capacity as high as 15 percent per week. Cathode potentials did not drop as before to 3.0 V (SC) or 3.3 V (Q), but remained near 4 V. Anode potentials quickly rose to >2.5 V versus  $\text{Li}^0$  upon storage. After-storage cycling revealed that cathode polarization increased rapidly from 50 mV initially to 300 mV after four weeks at 55 °C. Almost no change was observed in the anode polarization over the same period. A 2-V shift in the lithium reference potential was quite often found after one week of storage at 55 °C. Manganese was found on the lithium reference electrode, in the separator, and on the carbon anode by EDX after storage. These results were explained as another consequence of manganese dissolution from the spinel.

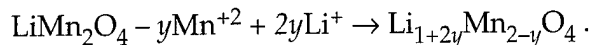
5. Manganese dissolution is given as the reason for increased cathode polarization, although a specific mechanism is not given.

SC and Q spinel samples were stored in 1-M  $\text{LiPF}_6$  in 2:1 EC/DMC at 55 °C for one to two months. Through AA, Mn was found in the supernatant; the SC sample showed more Mn dissolution than the Q sample. X-ray diffraction indicated the formation of a defect spinel, with increased Mn valence present after storage. This same defect spinel was found in cells stored at 55 °C for two weeks. SEM indicated pitting and

corrosion of spinel particles after storage at 55 °C. Electrochemical testing indicated that as storage at 55 °C was prolonged, capacity decreased and polarization increased, although fade behavior remained excellent. Again, these results were explained as another consequence of manganese dissolution from the spinel.

6. Manganese dissolution at the surface of a normal spinel particle causes the transformation of the outer layers into a defect spinel. This surface material is suggested to have low ionic/electronic conductivity and is responsible for the polarization seen in electrochemical measurements.

Blyr et al [26] proposed a chemical pathway to account for the observed manganese dissolution and increased cathode polarization. It is an ion exchange reaction between  $\text{Mn}^{+2}$  and  $\text{Li}^+$  that starts at the surface and proceeds toward the core of the particle:



One  $\text{Li}^+$  replaces a  $\text{Mn}^{+2}$  at a 16d site. An additional  $\text{Li}^+$  moves into the spinel structure and occupies a 16c site. The resulting material is a lithium-inserted, manganese-deficient spinel, with excess lithium in 16c octahedral sites. The excess lithium at the 16c sites results in a material with a 3-V potential, but increased manganese valence. This mechanism depends on the presence of  $\text{Mn}^{+2}$  at the spinel surface that can be exchanged for  $\text{Li}^+$ . This  $\text{Mn}^{+2}$  might be formed as a result of acid (HF) in the electrolyte catalyzing disproportionation of the surface  $\text{Mn}^{+3}$  into  $\text{Mn}^{+2}$  and  $\text{Mn}^{+4}$ .

### 3.3 After Storage

Du Pasquier et al [28] investigated storage of  $\text{Li}_{1.05}\text{Mn}_{1.95}\text{O}_4$  materials as a function of temperature, electrolyte composition, and spinel surface area. Spinel with surface areas ranging from 0.6 to 0.8  $\text{m}^2/\text{g}$  were synthesized when  $\text{Li}_2\text{CO}_3$  was reacted with EMD- $\text{MnO}_2$  at 800 °C, with repeated grinding and annealing followed by slow cooling. Spinel with larger surface areas of 5 to 6  $\text{m}^2/\text{g}$  were synthesized with  $\text{LiNO}_3$  instead of  $\text{Li}_2\text{CO}_3$  used as a precursor.  $\text{Li}_4\text{Mn}_5\text{O}_{12}$  was synthesized from  $\text{LiNO}_3$  and  $\gamma\text{-MnO}_2$  at 400 °C [29].  $\lambda\text{-MnO}_2$  was synthesized by acid etch [17] or by electrochemical delithiation.

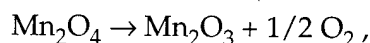
$\text{Li}_{1.05}\text{Mn}_{1.95}\text{O}_4$  stability was measured mainly at 55 and 100 °C. A typical experiment involved mixing 0.5 g of  $\text{LiMn}_2\text{O}_4$  powder with 10  $\text{cm}^3$  of 1-M  $\text{LiPF}_6$  in 1:1 w/w EC:DMC electrolyte. Variations on this experiment included the use of spinels with different surface areas and different electrolytes. These solutions were placed in either foil bags or Teflon™ bottles sealed in foil bags. After the appropriate time, samples were removed from their packaging in a drybox, and the aged spinel was separated from the electrolyte by centrifuge. Electrochemical measurements were conducted on Swagelok™-type cells and Bellcore PliON™ electrodes with 1-M  $\text{LiPF}_6$  in 1:1 w/w EC:DMC electrolyte.

Manganese dissolution was shown to increase as a function of temperature with as much as 15 percent manganese loss after 24 hr at 100 °C. With the dissolution mechanism operating at its highest rate at 100 °C, these samples were selected for further characterization. X-ray diffraction indicated that extra peaks were growing during storage. These extra peaks were identified with the phases  $\text{Li}_2\text{MnO}_3$ ,  $\lambda\text{-MnO}_2$ ,  $\text{Li}_4\text{Mn}_5\text{O}_{12}$ , and  $\text{Li}_2\text{Mn}_4\text{O}_9$ . When a higher-surface-area spinel was selected for 100 °C storage, the transformation of  $\text{Li}_{1.05}\text{Mn}_{1.95}\text{O}_4$  to  $\lambda\text{-MnO}_2$  was unambiguously indicated by x-ray diffraction. The variation in manganese and HF contents of the supernatant after storage indicates that manganese dissolution increases with increasing surface area, and that it is correlated to HF content—demonstrating that manganese dissolution is induced by acids.

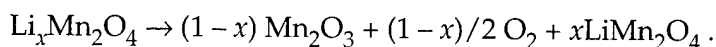
The effect of electrolyte on manganese dissolution was also studied.  $\text{LiPF}_6$  gave the highest manganese dissolution, with  $\text{LiBF}_4$ ,  $\text{LiAsF}_6$ , and  $\text{LiClO}_4$  showing lower manganese dissolution in EC:DMC electrolytes. Manganese dissolution was also lower in DEC-versus-EC-based electrolytes.

Infrared spectra of aged spinel samples washed with DMC indicate the presence of an organic layer surrounding the particle. The exact species making up this layer could not be identified and varied with electrolyte salt. Peak frequencies were indicative of C=O, C-O, C-C, Mn-O, and Li-O bonds, as well as  $\text{CH}_2$  and  $\text{CH}_3$  groups.

Thermogravimetric analysis (TGA) measurements on aged samples indicated  $\text{CO}_2$  release at 140 °C and  $\text{O}_2$  release at 500 °C. The  $\text{CO}_2$  is from the burning of the organic coating, and the  $\text{O}_2$  release is from the reaction



or



The oxygen loss is mainly seen in the  $\text{LiPF}_6$  electrolytes, showing that  $\lambda\text{-MnO}_2$  phase formation occurs more rapidly in this electrolyte than in the others studied.

A surface layer was observed from SEM measurements. The morphology of the spinel particles did not appear to change after 8 hr of aging, which discounted the possibility of a dissolution-recrystallization mechanism for  $\lambda\text{-MnO}_2$  phase formation. The passivation layer was suggested to be the source of polarization observed in  $\text{Li/LiMn}_2\text{O}_4$  cells. Water removed this surface layer, and subsequently the IR peaks and  $\text{CO}_2$  formation disappeared on heating. Gravimetric determinations before and after washing indicated that this passivation layer grew linearly with time. The passivating layer was also found to contain manganese and lithium; it was particularly rich in lithium.

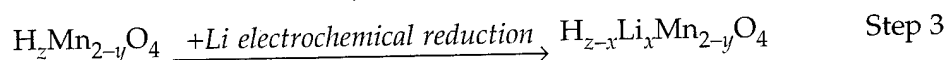
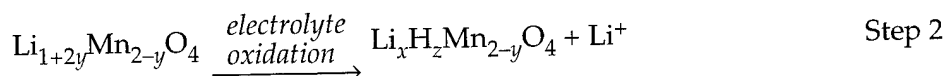
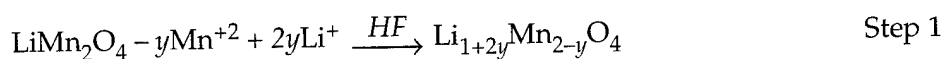


Washed samples were analyzed with Fourier transform infrared spectroscopy (FTIR) and found to contain absorption bands ascribed by Ammundsen et al [30,31] to lattice hydroxyl groups in manganese-deficient spinels of the general formula  $H_zMn_{2-y}O_4$ . Du Pasquier et al concluded that aging spinel in electrolyte at elevated temperature results in the formation of a protonated  $\lambda$ - $MnO_2$  phase covered with an organic passivating layer.

Electrochemical measurements were carried out on aged samples, either unwashed or washed with water. The initial open-circuit voltage increased from 3.8 to 4.2 V with storage time at 100 °C in the electrolyte. For the unwashed samples, a large polarization increase was observed with increasing storage time. The same effect, to a much smaller degree, was observed for the washed samples. For samples stored 1 to 2 hr and washed, almost all the capacity was recovered. For samples stored longer than this, permanent capacity loss was observed, along with modification of the voltage profile. This is indicative of a structural change and protonation of the structure to form  $H_zMn_{2-y}O_4$ -type materials. The presence of  $H_zMn_{2-y}O_4$  materials is significant, as these materials show lower capacity with respect to lithium insertion than  $\lambda$ - $MnO_2$ , due to the strong bonding between protons and the 16d manganese vacancies.

Similar results to the ones reported above were found for the electrochemically delithiated spinel, with solvent oxidation that was more pronounced due to the highly oxidizing nature of  $\lambda$ - $MnO_2$ .

Du Pasquier et al then proposed a fairly complete mechanism to account for capacity loss and rate capability loss on storage:



Step 1. Spinel undergoes cation exchange of  $Mn^{+2}$  for  $Li^+$  in acidic media. The mechanism creating  $Mn^{+2}$  is not specified, but is catalyzed by traces of acid.

Step 2. Manganese-deficient spinel undergoes proton exchange in the presence of  $H^+$  from electrolyte oxidation, creating a protonated  $\lambda$ - $MnO_2$ -type phase with a passivating film containing organic oxidation products, lithium, and manganese.

Step 3. Partial lithium intercalation of the protonated phase.

(The loss in rate capability results, therefore, from the formation of a passivating film on the spinel particle.)

## 4. Summary

A review of the literature suggests that loss in rate capability occurs in  $\text{LiMn}_2\text{O}_4$ /carbon cells as the result of several factors, all related to manganese dissolution:

- Manganese dissolution results in a loss of spinel particle contact and electrode polarization.
- Manganese dissolution at the surface of a normal spinel particle causes the transformation of the outer layers into a defect spinel. This surface material is suggested to have low ionic/electronic conductivity and is responsible for the polarization seen in electrochemical measurements.
- Manganese dissolution leads to the formation of a highly oxidizing, manganese-deficient material that further reacts with the electrolyte solvent and results in the formation of a rate-limiting, lithium-rich organic film.
- Manganese dissolution results in poisoning of the carbon anode and loss of its ability to cycle lithium.

## 5. Improving Rate Capability After Storage and During Cycling

Several solutions have been suggested to improve storage and cycling performance at elevated temperatures in the spinel/carbon lithium-ion battery:

- Decreasing manganese dissolution through modification of bulk properties and surface treatments.
- Increasing electrolyte stability to decrease acidification during storage and cycling.
- Removal of water and the use of chemical additives to trap protons.

Several of these proposed solutions are discussed in detail in this section.

### 5.1 Reduced Surface Area

The dissolution of manganese is said to occur at the surface of the spinel particle, as a result of attack from acids in the electrolyte. Reduction of the spinel surface area should therefore reduce manganese dissolution. Several researchers [20,25] have demonstrated the effect of surface area on manganese dissolution. The lowest surface areas reported, 0.5 to 0.6 m<sup>2</sup>/g, give the slowest manganese dissolution rates. This approach works to a point, beyond which reduction in surface area begins to affect rate capability due to diffusion limitations.

### 5.2 Surface Treatments

Amatucci et al [32] demonstrated the effectiveness of spinel surface treatments for reducing irreversible capacity loss. Several approaches were taken to modify the interface between the spinel particle and the electrolyte. The first was the coating of spinel particulates with a lithium boron oxide glass. The second was the complexation of surface manganese by acetylacetone.

Lithium boron oxide glasses were chosen for use as a coating because of their wettability toward the spinel and stability at high voltages, and because they are good solid ionic conductors. Li<sub>1.05</sub>Mn<sub>1.95</sub>O<sub>4</sub> was used as the base material onto which the glass was coated. The coatings were applied with either powder-coating or solution-evaporation techniques. The coated precursor materials were heated to 600 or 800 °C and slow-cooled to form the final product for testing. This coating resulted in

- no change in the spinel lattice parameter up to a 0.6 wt% coating,
- reduced catalytic activity toward oxidation of CO,
- reduction in surface area from 0.7 to 0.2 m<sup>2</sup>/g at 0.6 wt% coating, and

- reduced capacity loss on 55 °C storage, even in the presence of 500-ppm water spiked into the electrolyte.

The effectiveness of the lithium borate glass treatment was not directly tied to manganese dissolution through measurements of manganese in the solution. The improvement in 55 °C storage performance was said to result from either lowered surface area or lowered activity toward electrolyte oxidation.

Acetylacetone (a well-known chelating agent) is used to remove active manganese sites from the surface of spinel particles.  $\text{Li}_{1.05}\text{Mn}_{1.95}\text{O}_4$  was stirred in acetylacetone for various amounts of time, washed with acetone, and heated to 800 °C, followed by slow cooling. The treatment resulted in removal of manganese from the spinel as monitored by AA. The final coating resulted in

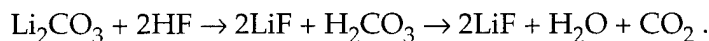
- reduced catalytic activity toward the oxidation of CO,
- reduction in surface area from 0.7 to 0.5 m<sup>2</sup>/g after 24 hr of treatment, and
- reduced capacity loss on 55 °C storage.

Amatucci et al proposed that the improvement in 55 °C storage performance resulted from the formation of a manganese-deficient material, possibly  $\text{Li}_2\text{MnO}_3$ , at the surface of the spinel due to manganese removal by acetylacetone. This would result in a surface layer containing only  $\text{Mn}^{+4}$ , which is more resistant to dissolution. This would be consistent with the results of Yamamoto et al [33].

### 5.3 Trapping HF/Water Removal

Several researchers [21,32] have demonstrated the effect of water contamination on manganese dissolution in spinel lithium-ion batteries. Water is removed by drying of the electrolyte solvents, salts, and cell components. Unfortunately, the most often used salt ( $\text{LiPF}_6$ ) in lithium-ion batteries always has traces of HF from the manufacturer.

Materials such as  $\text{Li}_2\text{CO}_3$  can trap acid present in the lithium-ion battery:



This material is not very useful in practice—because it produces  $\text{H}_2\text{CO}_3$ , which decomposes to  $\text{CO}_2$  and water, which then reacts with  $\text{LiPF}_6$ —but it does demonstrate the concept of proton trapping.

## 6. Conclusions

Loss in rate capability occurs during cycling and in storage in both the charged and discharged states. This loss in rate capability is the result of manganese dissolution, which leads to the following effects:

- loss of spinel particle contact,
- transformation of the spinel surface to a material with low ionic/electronic conductivity,
- formation of a highly oxidizing manganese-deficient material that reacts with the electrolyte solvent and results in the formation of a rate-limiting, lithium-rich organic film, and
- passivation of the carbon anode by manganese.

Manganese dissolution can be reduced through

- modification of bulk properties and surface treatments,
- increase in electrolyte stability, and
- removal of water and the use of additives to trap protons.

Further research is needed to reduce manganese dissolution in  $\text{LiMn}_2\text{O}_4$ .

## References

1. J. M. Tarascon, E. Wang, F. K. Shokoohi, W. R. McKinnon, and S. Colson, *J. Electrochem. Soc.* **138**, 2859 (1991).
2. T. Ohzuku, M. Kitagawa, and T. Hirai, *J. Electrochem. Soc.* **137**, 769 (1990).
3. M. M. Thackeray, P. J. Johnson, L. A. de Picciotto, P. G. Bruce, and J. B. Goodenough, *Mater. Res. Bull.* **19**, 179 (1984).
4. M. Winter, J. O. Besenhard, M. E. Spahr, and P. Novák, *Adv. Mater.* **10**, 725 (1998).
5. D. G. Wickham and W. J. Croft, *J. Phys. Chem. Solids* **7**, 351 (1958).
6. P. Barboux, J. M. Tarascon, and F. K. Shokoohi, *J. Solid State Chem.* **94**, 185 (1991).
7. W. Liu, K. Kowal, and G. C. Farrington, *J. Electrochem. Soc.* **143**, 3590 (1996).
8. F. K. Shokoohi, J. M. Tarascon, B. J. Wilkens, D. Guyomard, and C. C. Chang, *J. Electrochem. Soc.* **139**, 1845 (1992).
9. M. M. Thackeray, A. de Kock, M. H. Rossouw, D. Liles, R. Bittihn, and D. Hoge, *J. Electrochem. Soc.* **139**, 363 (1992).
10. T. Tsumura, A. Shimizu, and M. Inagaki, *Solid State Ionics* **90**, 197 (1996).
11. V. Manev, A. Momchilov, A. Nassalevka, and A. Kozawa, *J. Power Sources* **41**, 305 (1993).
12. J. M. Tarascon, W. R. McKinnon, F. Coowar, T. N. Bowmer, G. Amatucci, and D. Guyomard, *J. Electrochem. Soc.* **141**, 1421 (1994).
13. A. de Kock, M. H. Rossouw, L. A. de Picciotto, M. M. Thackeray, W.I.F. David, and R. M. Ibberson, *Mater. Res. Bull.* **25**, 657 (1990).
14. R. J. Gummow, A. de Kock, and M. M. Thackeray, *Solid State Ionics* **69**, 59 (1994).
15. A. Yamada, K. Miura, K. Hinokuma, and M. Tanaka, *J. Electrochem. Soc.* **142**, 2149 (1995).
16. Y. Gao and J. R. Dahn, *J. Electrochem. Soc.* **143**, 100 (1996).
17. J. Hunter, *J. Solid State Chem.* **39**, 142 (1981).
18. M. M. Thackeray, W.I.F. David, P. G. Bruce, and J. B. Goodenough, *Mat. Res. Bull.* **18**, 461 (1983).
19. Y. Gao and J. R. Dahn, *Solid State Ionics* **84**, 33 (1996).
20. D. H. Jang, Y. J. Shin, and S. M. Oh, *J. Electrochem. Soc.* **143**, 2204 (1996).
21. D. H. Jang, and S. M. Oh, *J. Electrochem. Soc.* **144**, 3342 (1997).
22. J. M. Tarascon, U.S. Patent 5,425,932 (1995).

23. D. Guyomard and J. M. Tarascon, *J. Electrochem. Soc.* **140**, 3071 (1993).
24. D. Guyomard and J. M. Tarascon, *Solid State Ionics* **69**, 222 (1994).
25. G. G. Amatucci, C. N. Schmutz, A. Blyr, C. Sigala, A. S. Gozdz, D. Larcher, and J. M. Tarascon, *J. Power Sources* **69**, 11 (1997).
26. A. Blyr, C. Sigala, G. Amatucci, D. Guyomard, Y. Chabre, and J. M. Tarascon, *J. Electrochem. Soc.* **145**, 194 (1998).
27. T. Gozdz, C. Schmutz, and J. M. Tarascon, U.S. Patent 5,296,318 (1996).
28. A. Du Pasquier, A. Blyr, P. Courjal, D. Larcher, G. Amatucci, B. Gérard, and J. M. Tarascon, *J. Electrochem. Soc.* **146**, 428 (1999).
29. M. M. Thackeray, M. F. Mansuetto, D. W. Dees, and D. R. Vissers, *Mater. Res. Bull.* **31**, 133 (1996).
30. B. Ammundsen, G. R. Burns, D. J. Jones, and J. Roziere, *Chem. Mater.* **7**, 2151 (1995).
31. B. Ammundsen, P. B. Aitchison, G. R. Burns, D. J. Jones, and J. Roziere, *Solid State Ionics* **97**, 269 (1997).
32. G. G. Amatucci, A. Blyr, C. Sigala, P. Alfonse, and J. M. Tarascon, *Solid State Ionics* **104**, 13 (1997).

## Distribution

Admnstr  
Defns Techl Info Ctr  
Attn DTIC-OCF  
8725 John J Kingman Rd Ste 0944  
FT Belvoir VA 22060-6218

Ofc of the Secy of Defns  
Attn ODDRE (R&AT)  
The Pentagon  
Washington DC 20301-3080

Ofc of the Secy of Defns  
Attn OUSD(A&T)/ODDR&E(R) R J Trew  
3080 Defense Pentagon  
Washington DC 20301-7100

Advry Grp on Elect Devices  
Attn Documents  
Crystal Sq 4 1745 Jefferson Davis Hwy Ste 500  
Arlington VA 22202

AMCOM MRDEC  
Attn AMSMI-RD W C McCorkle  
Redstone Arsenal AL 35898-5240

CECOM Night Vsn/Elect Sensors Dirctr  
Attn AMSEL-RD-NV-D  
FT Belvoir VA 22060-5806

Commander  
CECOM R&D  
Attn AMSEL-IM-BM-I-L-R Stinfo Ofc  
Attn AMSEL-IM-BM-I-L-R Techl Lib  
FT Monmouth NJ 07703-5703

Deputy for Sci & Techlgy  
Attn Ofc Asst Sec Army (R&D)  
Washington DC 30210

Dir for MANPRINT  
Ofc of the Deputy Chief of Staff for Prsnl  
Attn J Hiller  
The Pentagon Rm 2C733  
Washington DC 20301-0300

Hdqtrs  
Attn DAMA-ARZ-D F D Verderame  
Washington DC 20310

US Army ARDEC  
Attn AMSTA-AR-TD M Fisette  
Bldg 1  
Picatinny Arsenal NJ 07806-5000

Commander  
US Army CECOM  
Attn AMSEL-RD-CZ-PS-B M Brundage  
FT Monmouth NJ 07703-5000

US Army CECOM Rsrch Dev & Engrg Ctr  
Attn AMSEL-RD-AS-BE E Plichta  
FT Monmouth NJ 07703-5703

US Army Info Sys Engrg Cmnd  
Attn ASQB-OTD F Jenia  
FT Huachuca AZ 85613-5300

US Army Natick RDEC Acting Techl Dir  
Attn SSCNC-T P Brandler  
Natick MA 01760-5002

US Army Simulation, Train, & Instrmntn  
Cmnd  
Attn J Stahl  
12350 Research Parkway  
Orlando FL 32826-3726

US Army Soldier & Biol Chem Cmnd Dir of  
Rsrch & Techlgy Dirctr  
Attn SMCCR-RS I G Resnick  
Aberdeen Proving Ground MD 21010-5423

US Army Tank-Automtv Cmnd Rsrch, Dev, &  
Engrg Ctr  
Attn AMSTA-TR J Chapin  
Warren MI 48397-5000

US Army Train & Doctrine Cmnd  
Battle Lab Integration & Techl Dirctr  
Attn ATCD-B J A Klevecz  
FT Monroe VA 23651-5850

US Military Academy  
Mathematical Sci Ctr of Excellence  
Attn MDN-A LTC M D Phillips  
Dept of Mathematical Sci Thayer Hall  
West Point NY 10996-1786



## Distribution (cont'd)

Nav Rsrch Lab  
Attn Code 2627  
Washington DC 20375-5000

Nav Surface Warfare Ctr  
Attn Code B07 J Pennella  
17320 Dahlgren Rd Bldg 1470 Rm 1101  
Dahlgren VA 22448-5100

Marine Corps Liaison Ofc  
Attn AMSEL-LN-MC  
FT Monmouth NJ 07703-5033

USAF Rome Lab Tech  
Attn Corridor W Ste 262 RL SUL  
26 Electr Pkwy Bldg 106  
Griffiss AFB NY 13441-4514

DARPA  
Attn S Welby  
3701 N Fairfax Dr  
Arlington VA 22203-1714

Hicks & Associates Inc  
Attn G Singley III  
1710 Goodrich Dr Ste 1300  
McLean VA 22102

Palisades Inst for Rsrch Svc Inc  
Attn E Carr  
1745 Jefferson Davis Hwy Ste 500  
Arlington VA 22202-3402

Director  
US Army Rsrch Ofc  
Attn AMSRL-RO-D JCI Chang  
Attn AMSRL-RO-EN W D Bach  
Attn AMSRL-RO-EN B Mann  
PO Box 12211  
Research Triangle Park NC 27709

US Army Rsrch Lab  
Attn AMSRL-DD J M Miller  
Attn AMSRL-CI-AI-A Mail & Records Mgmt  
Attn AMSRL-CI-AP Techl Pub (3 copies)  
Attn AMSRL-CI-LL Techl Lib (3 copies)  
Attn AMSRL-DC T Wolfenstine  
Attn AMSRL-SE-D E Scannell  
Attn AMSRL-SE-DC D Foster  
Attn AMSRL-SE-DC J Read (10 copies)  
Attn AMSRL-SE-DC S Gilman  
Attn AMSRL-SE-DC W Behl  
Attn AMSRL-SE-E J Mait  
Adelphi MD 20783-1197

|  |  |   |  |  |
|--|--|---|--|--|
| <b>REPORT DOCUMENTATION PAGE</b>   |  |   | Form Approved<br>OMB No. 0704-0188                         |  |
| Public reporting burden for this collection of information is estimated to average 1 hour per response, including the time for reviewing instructions, searching existing data sources, gathering and maintaining the data needed, and completing and reviewing the collection of information. Send comments regarding this burden estimate or any other aspect of this collection of information, including suggestions for reducing this burden, to Washington Headquarters Services, Directorate for Information Operations and Reports, 1215 Jefferson Davis Highway, Suite 1204, Arlington, VA 22202-4302, and to the Office of Management and Budget, Paperwork Reduction Project (0704-0188), Washington, DC 20503. |  |   |  |  |
| 1. AGENCY USE ONLY (Leave blank)   |  | 2. REPORT DATE<br>March 2000                                |  | 3. REPORT TYPE AND DATES COVERED<br>Summary, 9/98-9/99     |
| 4. TITLE AND SUBTITLE<br>Loss of Rate Capability in LiMn <sub>2</sub> O <sub>4</sub> /Carbon Cells   |  |   | 5. FUNDING NUMBERS<br>DA PR: N/A<br>PE: 62120A             |  |
| 6. AUTHOR(S)<br>Jeffrey Read, Jeff Wolfenstine, Donald Foster, and Wishvender Behl   |  |   |  |  |
| 7. PERFORMING ORGANIZATION NAME(S) AND ADDRESS(ES)<br>U.S. Army Research Laboratory<br>Attn: AMSRL-SE-DC email: jef_wolfenstine@stinger.arl.mil<br>2800 Powder Mill Road<br>Adelphi, MD 20783-1197   |  |   | 8. PERFORMING ORGANIZATION<br>REPORT NUMBER<br>ARL-TR-2115 |  |
| 9. SPONSORING/MONITORING AGENCY NAME(S) AND ADDRESS(ES)<br>U.S. Army Research Laboratory<br>2800 Powder Mill Road<br>Adelphi, MD 20783-1197  |  |   | 10. SPONSORING/MONITORING<br>AGENCY REPORT NUMBER          |  |
| 11. SUPPLEMENTARY NOTES<br>ARL PR: 9N0V VV<br>AMS code: 622120.H16   |  |   |  |  |
| 12a. DISTRIBUTION/AVAILABILITY STATEMENT<br>Approved for public release;<br>distribution unlimited.  |  |   | 12b. DISTRIBUTION CODE                                     |  |
| 13. ABSTRACT (Maximum 200 words)<br>We present a survey of the available literature on the loss in rate capability of LiMn <sub>2</sub> O <sub>4</sub> -based lithium-ion batteries. Manganese dissolution is identified as the main cause of rate capability loss, as well as loss in capacity during storage. Manganese dissolution results in passivation of both the cathode and anode, structural changes at the spinel surface, and loss in particle contact. Manganese dissolution can be reduced by surface treatments, increased electrolyte stability, and removal of acidic protons from the electrolyte.   |  |   |  |  |
| 14. SUBJECT TERMS<br>Lithium manganese oxide, spinel   |  |   | 15. NUMBER OF PAGES<br>26                                  |  |
|  |  |   | 16. PRICE CODE   |  |
| 17. SECURITY CLASSIFICATION<br>OF REPORT<br>Unclassified   |  | 18. SECURITY CLASSIFICATION<br>OF THIS PAGE<br>Unclassified |  | 19. SECURITY CLASSIFICATION<br>OF ABSTRACT<br>Unclassified |
|  |  |   |  | 20. LIMITATION OF ABSTRACT<br>UL                           |